Charge density and plasmon modes in a triangular quantum well model for doped and undoped gated AlGaN/GaN HEMTs

S Rabbaa, J Stiens

Charge density and plasmon modes in a triangular quantum well model for doped and undoped gated AlGaN/GaN HEMTs

S Rabbaa and J Stiens

Laboratory of Micro- and PhotonElectronics, Dept. of Electronics and Informatics, Vrije Universiteit Brussel, Pleinlaan 2, 1050-Brussels, Belgium.

E-mails: srabbaa@etro.vub.ac.be ; jstiens@etro.vub.ac.be

Abstract. We have calculated the plasmon frequency of the two-dimensional electron gas (2DEG) in AlGaN/GaN high electron mobility transistors (HEMT). The impact of HEMT's parameters on the plasmon frequency and the sheet charge density of the 2DEG is discussed in detail. The charge density in the HEMT's channel is calculated by means of a triangular quantum well (TQW) model. It has been found that the AlGaN/GaN heterostructure induces plasmon oscillations in the THz range with larger frequencies compared to other semiconductor compounds. The sensitivity of the tunability of these frequencies is considerable, especially by using a variable applied gate voltage. We have derived optimal structure parameters for obtaining a maximum plasmon frequency for a given doping concentration. We will show that the accuracy of this optimized frequency value is dependent on the average position Δd of charge density in the triangular shaped (quantum well) channel. The interaction between radiation and plasmons has many applications such as detectors, mixers and generators of THz waves.

Keywords: Plasmon frequency, 2DEG, HEMT, AlGaN/GaN heterostructure, sheet charge density, THz.

1. Introduction

During the last decade of the 21th century, considerable progress had been made in the technology of gallium nitride (GaN) based HEMTs. GaN has unique properties that make it an attractive electronic and optoelectronic material. It is optically transparent and it has exceptional chemical and physical stability. It is used in biosensors fabrication due to its properties of non- toxic surface content (like As) and the immobilization of bio-molecules [1]. The AlGaN/GaN based HEMTs have some advantages that make it outperform upon other heterostructures. Some of these features are: introducing high density 2DEG, high current density, high carrier mobility, low sheet resistance and high transconductance [2]. The sheet charge density can become an order of magnitude larger (as we will see) than in GaAs/AlGaAs heterostructures which provides a plasmon frequency about 3 times larger.

The frequency response of the two-dimensional (2D) electron channel in HEMTs is affected by the excitation of plasma oscillations of the 2DEG under the gate electrode [3]. The coupling mechanism between 2D plasmons and external electromagnetic waves were discussed in [4-7]. It was suggested that this coupling might be stronger using the design of field effect transistors array with grating gates [8]. This excitation mechanism allows for the design of THz tunable detectors and generators. The plasmon oscillation in 2D promotes effective emission of THz radiation [8]. The use of THz spectrum in the sensing of chemical and biological systems and in the detection of hidden weapons and mines requires high sensitive and fast response detectors. THz emitters and detectors are used in medical, biological and industrial imaging, communications and space sciences [1,9]. The plasmon frequency of the 2DEG in AlGaN/GaN based HEMT belongs to the THz gap and it can exceed 10 THz

compared to the low band of THz frequency range in conventional classical semiconductor devices such as tunneling diodes and classical transistors [10].

After giving a short overview of the various expressions of the plasmon frequency in various (gated) structures and its relation to the charge density, our structure is introduced in section 3 with a description of the induced polarizations in its channel. Our focus is laid upon the design parameters and the analysis of TQW in section 4. Calculations and discussions are presented in section 5.

2. Plasmon Frequency in 2DEG System

The frequency of plasmon oscillations in three-dimensional (3D) materials is given by:

$$\omega_p^2 = \frac{e^2 N}{\varepsilon_o \varepsilon_\infty m^*} \qquad (\text{rad}^2/\text{s}^2) \qquad (1)$$

with N the free carrier concentration, e the electron charge ,m^* the electron effective mass, ε_∞ the high frequency dielectric constant and ε_o the vacuum permittivity. The phonon-plasmon coupling and the interaction between plasmons and THz radiation in bulk GaN was discussed in [1]. The 3D plasmon frequency in highly doped GaN has THz applications even in the range of CO_2 laser radiation.

Plasmon oscillations in 2D electron system were introduced by Stern [11] and they were observed experimentally in a sheet of electrons in liquid helium [12] and in silicon metal-insulator-semiconductor structures [13]. There are two types of excited plasma waves in HEMTs: gated (screened) plasmons and un-gated (unscreened) plasmons. The spectrum of the gated plasmon modes which are excited under the gate contact is given by:

$$\omega_p^2 = \frac{e^2 N_s k}{m^* \varepsilon_o [\varepsilon_s + \varepsilon_b \coth(kd)]} \qquad (\text{rad}^2/\text{s}^2) \qquad (2)$$

where N_s is the sheet carrier concentration at the heterostructure interface, k is the plasmon wavevector, ε_s , ε_b are the dielectric constants of surrounding materials (substrate and barrier materials, respectively) , and d is the distance between gate plane and the 2D electron channel [8]. The wavevector is given by $k = \pi n / (L+2d)$, where n=1, 2, 3..., and L is the gate length. When n is even, plasmon modes of the charge density under the gate cannot be excited with THz radiation due to zero net dipole moment of the modes. Therefore, to get odd modes, the wavevector should be taken as $k= (2n-1)\ \pi/L$. If kd << 1, 'equation 2' can be written as:

$$\omega_p^2 = \frac{e^2 N_s d}{\varepsilon_o \varepsilon_b m^*} k^2 \qquad (3)$$

If the barrier layer is thin compared to the gate length (d<<L), then the first harmonic of plasmon oscillations with n=1 (the fundamental plasmon mode) can be given in terms of the gate voltage (V_g) and threshold voltage (V_{th}) as:

$$\omega_p^2 = \frac{e\,(V_g - V_{th})}{m^*} k^2 \qquad (4)$$

Although it may be possible to achieve large THz plasmon frequencies by decreasing the gate length, there are actually some limitations in designing HEMTs with very short gate lengths. According to 'equation 4', the modes excited under the gate electrode can be tuned by changing V_g, and so they have more practical applications than un-gated modes [8].

3. Induced polarization in AlGaN/GaN heterostructure

A cross section of a HEMT is shown in 'figure 1'. The epitaxial layers are usually grown by various techniques such as molecular beam epitaxy (MBE), Metalorganic vapor phase epitaxy (MOVPE) and metalorganic chemical vapor deposition (MOCVD) on a substrate, typically

sapphire or SiC. The growth sequence is: undoped GaN buffer layer of thickness 0.6-3 μm (typically 1 μm, followed by undoped i-AlGaN spacer layer of thickness d_i between 0-10 nm, and finally a doped AlGaN layer of thickness d_n. The purpose of the spacer layer is to reduce Coulombic scattering caused by electrical interaction between the electrons in the 2DEG and ionized donors in the doped AlGaN layer, which will increase the electron mobility [14]. A 2DEG of average position Δd from the heterointerface is formed at the heterostructure of the buffer and spacer layers.

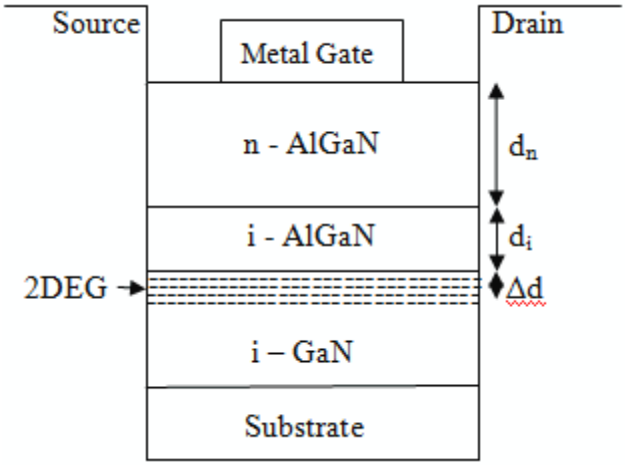

'Figure 1': Schematic diagram of AlGaN/GaN HEMT structure.

A high charge is induced in the channel even if the upper layer of AlGaN is undoped or/and without external electric field (V_g=0). This is one of the AlGaN/GaN heterostructure properties and advantages over other heterojunctions. In this case there are two types of macroscopic polarizations [15]:

- Spontaneous polarization (P_{sp}): due to the cation and anion positions in the lattice. It is given in terms of the Al-mole fraction (x) as:

$$P_{sp} = -0.090\,x - 0.034\,(1-x) + 0.019\,x\,(1-x) \qquad (\mathrm{C/m^2}) \qquad (5)$$

- Piezoelectric polarization (P_{pz}): due to lattice mismatch between GaN and AlGaN layers. It is given using Vegard's law by:

$$P_{pz}^{AlGaN} = xP_{pz}^{AlN} + (1-x)P_{pz}^{GaN} \qquad (6)$$

where P_{pz}^{AlN} and P_{pz}^{GaN} are given in terms of the strain ∈ as:

$$P_{pz}^{AlN} = -1.808 \in -7.888\ \in^2 \qquad (7)$$

$$P_{pz}^{GaN} = -0.918 \in +9.541\ \in^2 \qquad (8)$$

Nitride wafers are generally grown along the c-axis, and as a result the strain exits onto the epitaxial layer in the basal plane, and it is given by:

$$\in (x) = \frac{a_o - a(x)}{a(x)} \quad (9)$$

where a(x) = 0.31986 -0.00891 x is the lattice constant of AlGaN, and a_o= a(x =0) is the lattice constant of GaN.

The above expressions give the two polarizations as a quadratic equation of x (nonlinear polarization). It was found experimentally [15, 16] that the nonlinear model is more accurate than linear ones which were considered in some research works.

4. The sheet charge concentration

The total polarization (σ) induced at the heterostructure is related to P_{sp} and P_{pz} of the two layers forming the heterostructure by the following equation [17]:

$$\sigma(x) = P_{pz}^{AlGaN} + P_{sp}^{AlGaN} - P_{sp}^{GaN} \quad (10)$$

where we consider $P_{pz}^{GaN} \approx 0$ because its thickness is much larger than the strained AlGaN layer, and so it is fully relaxed. The free charge carriers are assumed approximately to occupy a triangular quantum well which contains a constant built-in electric field [18, 19]. To find the energy states and the population of free electrons in each energy state, we have solved Schrodinger's equation for the TQW. A detailed solution can be found in [20]. The energy eigenvalues are given by:

$$E_j = \left(\frac{\hbar^2}{2m^*}\right)^{1/3} \left[\frac{3\pi e \mathcal{F}_{eff}}{2}\left(j + \frac{3}{4}\right)\right]^{2/3} \qquad \text{j=0,1,2…} \quad (11)$$

We are interested in the first two energy states: E_o, the ground state, and E_1, the first excited state. For undoped or lowly doped heterostructures, $\mathcal{F}_{eff} = \mathcal{F}_s$, while for highly doped case, the effective electric field is $\mathcal{F}_{eff} = \mathcal{F}_s/2$, where the surface field $\mathcal{F}_s = eN_s/\varepsilon_s$, with ε_s the dielectric constant of GaN and N_s the charge density at the heterostructure given by [20]:

$$N_s = Dk_BT \sum_{j=0}^{1} ln\left[1 + exp\left(\frac{E_F - E_j}{k_BT}\right)\right] = Dk_BT\, ln\left\{\left[1 + exp\left(\frac{E_F - E_0}{k_BT}\right)\right]\left[1 + exp\left(\frac{E_F - E_1}{k_BT}\right)\right]\right\} \quad (12)$$

where $D=m^*/\pi\hbar$ is the conduction band density of states of the 2D system, k_B is Boltzmann's constant, T is the absolute temperature and E_F is the Fermi energy.

When two different semiconductors (like GaN and AlGaN) form a heterostructure, charges transfer across the interface until the Fermi energy on both sides are equal, because the surface depletion layer and heterojunction interface depletion regions overlap. Therefore, electrons are transferred from the ionized donors in doped AlGaN layer to the conduction band. Thus, the GaN layer at the interface is populated by transferred charges from the barrier and the polarization induced charged at the heterointerface as discussed in section 3. If we assume complete depletion of the AlGaN barrier, taking into account the polarization effect and the applied gate potential, then the charge density concentration at the AlGaN/GaN heterointerface can be obtained by solving the one dimensional Poisson's equation, and it is given as [21, 22]:

$$N_s = \frac{\varepsilon(x)}{e(d_n + d_i + \Delta d)}\left(V_g - V_{th} - V_c - \frac{E_F}{e}\right) \quad (13)$$

where $\varepsilon(x)$ = 9.5-0.5 x is the dielectric constant of $Al_xGa_{1-x}N$, V_c is the channel potential at a certain distance from the source due to drain source potential, and it can be obtained in [23]. The 2DEG average position Δd from the heterointerface can be calculated from the weighted average position of all energy levels [24]:

$$\Delta d = \frac{\frac{2}{3}\sum_j N_{sj} d_j}{N_s} \tag{14}$$

where N_{sj} and d_j are the charge density and average distance of carriers in the jth subband, respectively, and N_s is the total carrier concentration. Using Fermi-Dirac statistical functions to determine the population charge N_{sj}, we find that N_{so} (ground state) >> N_{s1} (first excited state). Thus $\Delta d = 2E_o/3e\mathcal{F}_{eff}$ [25]. The threshold voltage is given by:

$$V_{th}(x) = \phi_b - \frac{\Delta E_c}{e} - \frac{eN_d d_n^2}{2\varepsilon(x)} - \frac{|\sigma(x)|}{\varepsilon(x)}(d_n + d_i) \tag{15}$$

where ϕ_b=1.3 x +0.84 is the Schottky barrier, ΔE_c=0.7 [$E_g(x)$-$E_g(0)$] is the conduction band discontinuity between AlGaN and GaN, with E_g=6.13 x +3.42(1- x)-x(1- x) is the band gap of AlGaN, and N_d is the doping concentration in the barrier ($\varepsilon(x)$, ϕ_b, ΔE_c , and E_g are taken from [17]).

5. Results and discussions

As it is clear in 'equation 2', the plasmon frequency depends on the HEMT parameters and on the sheet charge density which is a function of the gate voltage. We can control required values of N_s (and then ω_p) by changing the quantities appearing in 'equations 12 and 13', which are: m*, ε (they depend on the type of material), d_i, d_n, N_d, x and V_g. Therefore, we have firstly calculated numerically the sheet charge density at different quantities of the previous independent variables. Because we have a function of many variables, then we plot the relationship with one independent variable and all other variables are fixed. All calculations are taken at temperature T=300 K, and at spacer layer thickness d_i=3 nm and V_c=0.

Solving 'equations 12 and 13' simultaneously leads to an implicit relationship between N_s and the other variables. 'Figure 2' shows the relationship between charge density and gate voltage for doped and undoped heterostructures. The curves consist of two parts: the first is at Vg < V_{th} (N_s=0) and the second is at Vg > V_{th} (inclined lines). The slope of each line is related to the capacitance of the structure. For the doped case, the slopes are 2.42×10^{12} $cm^{-2}V^{-1}$, 1.95×10^{12} $cm^{-2}V^{-1}$ and 1.66×10^{12} $cm^{-2}V^{-1}$ at d_n=15, 20, and 25 nm, respectively. We notice that the slopes, and then the capacitance, are

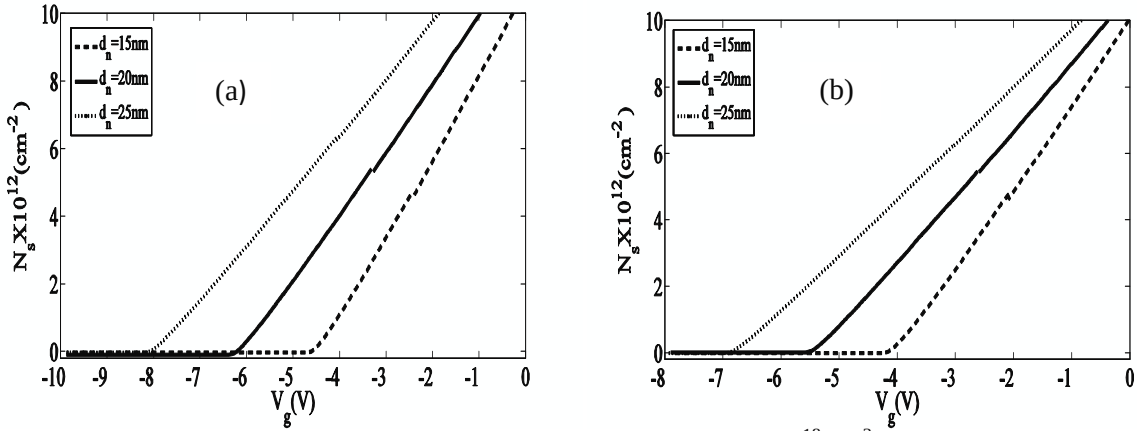

'Figure 2': Sheet charge density vs gate voltage at x=0.3, (a) $N_d=2\times10^{18}cm^{-3}$ and (b) undoped structure.

inversely proportional with the barrier layer thickness which increases the distance between the gate and the channel. What is interesting to note is that we have large charge density even in an undoped structure. This is because of the large contribution of the induced polarization (which doesn't depend on N_d) to the total sheet charge density. Therefore, it is possible to design AlGaN/GaN HEMT without the need to have a doped barrier.

The magnitude of the threshold voltage (absolute value) is increasing with the increase of barrier thickness as shown in 'figure 2'. This is because we have larger ionized charges and they need more gate voltage to be depleted to the channel.

The relationship between charge density and barrier layer thickness at different doping concentrations is shown in 'figure 3'. The change of charge density with doping concentration at different gate voltage is shown in 'figure 4'. We notice that the charge density is directly proportional with d_n and N_d because the quantity of diffused ionized impurities from the barrier to the charge channel increase with the increase of doping concentration or/and barrier thickness. The slopes of tangents in 'figure 3' for

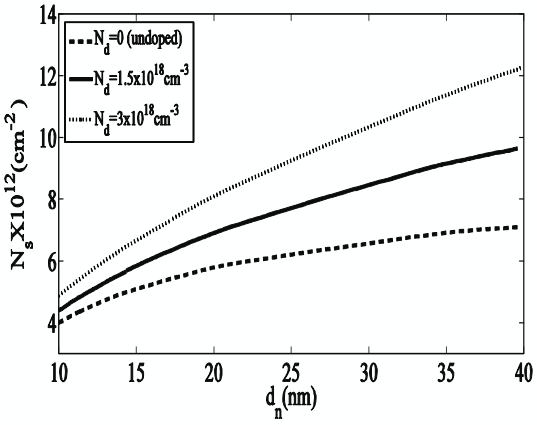

'Figure 3': Sheet charge density vs barrier layer thickness at x=0.2 and V_g=0.

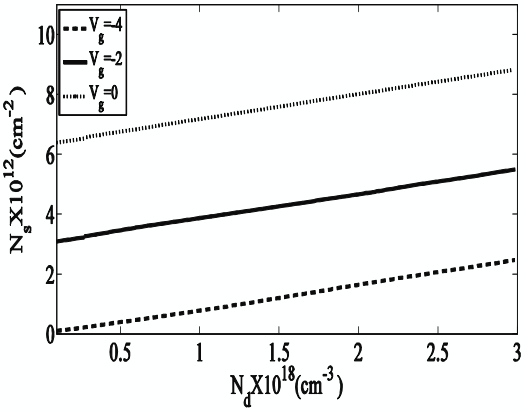

'Figure 4': Sheet charge density vs doping concentration at x=0.2 and d_n=25 nm.

each curve are larger as N_d increases. This makes the change of the sheet charge density with barrier thickness more sensitive in case of higher doping density. It is obvious in 'figure 3' that we can get the same value of N_s by choosing large d_n with small N_d or small d_n with large N_d. The first choice is better

because it gives lower capacitance and it reduces the effect of deep donors. However, it is important to maintain the barrier thickness d_n below the critical value for strain relaxation.

The variation of charge density with Al–mole fraction is shown in 'figure 5'. We include the induced polarization charge (σ) in the figure which is higher in case of AlGaN/GaN heterostructures compared to other semiconductors. The polarization features a non-linear dependence on x. It is increasing directly with x because it depends on the pseudomorphic strain which is a measure of the degree of lattice mismatch between AlGaN and GaN layers. The lattice mismatch increases with x. The sheet charge density increases with x because it depends on σ which has the major impact on N_s.

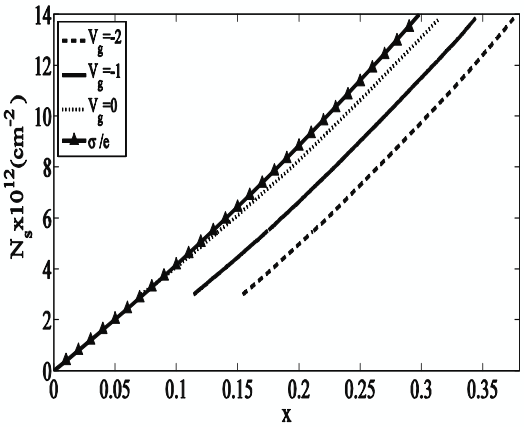

'Figure 5': Sheet charge density vs Al–mole fraction at d_n=25 nm and N_d=2×10^{18}cm^{-3}.

We will discuss now the dependance of the plasmon frequency on the variables mentioned above. The impact of gate voltage on the plasmon frequency is shown in 'figure 6'. For a certain HEMT which has been manufactured, its parameters (such as x, d_n and N_d) can't be changed because they are internal properties. What we can do is the change of V_g (external parameter) to control the desired value of ω_p. 'Figure 6' shows high sensitivity of the plasmon frequency to gate voltage. For example at d_n= 15 nm, the sensitivity is 2.98, 1.40 and 0.82 THz /V at -4.7<V_g<-4, -4<V_g<-2 and -2<V_g<2, respectively. This demonstrates why the gated plasmons have more practical applications than ungated modes.

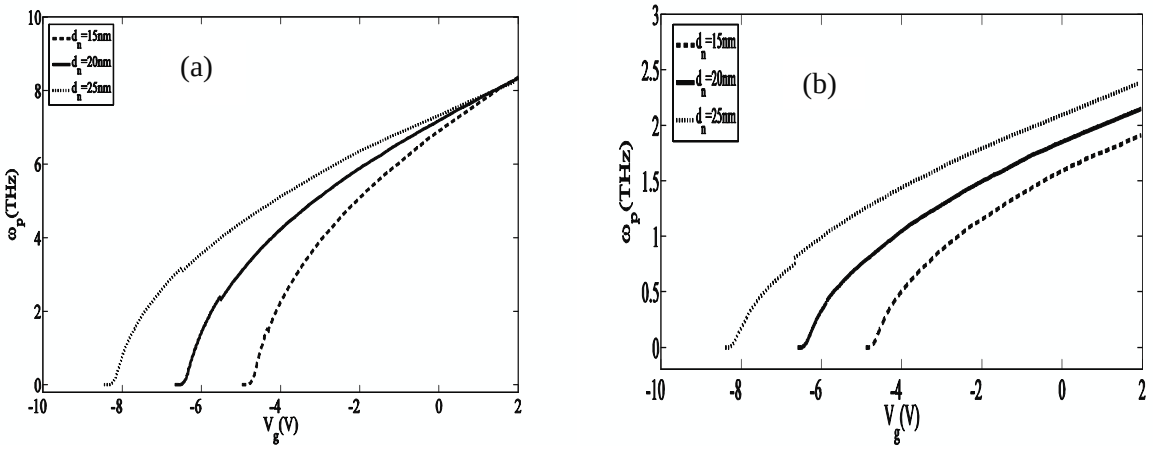

'Figure 6': Plasmon frequency vs gate voltage at x=0.3, N_d=2×10^{18} cm^{-3},(a) L= 60 nm,(b) L=500 nm

'Figure 7' shows the relation between plasmon frequency and barrier thickness at different doping densities. We notice clearly a maximum value of ω_p for the undoped case in (a), and it will appear in all curves if we mathematically increase d_n. This is an interesting optimization which can be obtained by means of the material and geometrical parameters. It is necessary to emphasize that the accuracy of the optimized value is controlled by taking into account the average position Δd of charge density in the channel. Many papers neglect the impact of Δd on N_s (and as a result on the sensitivity of ω_p). Although Δd is relatively small (1.7-8.0 nm), it will be considerable when d_n is small enough. As it is clear in 'equation 13', the charge density depends on the total distance of its position from the gate ($=d_n+d_i+\Delta d$). By increasing d_n, N_s increases (see 'figure 3'), while k decreases. Therefore, according to 'equation 2' the effect of N_s dominates the effect of k on the Plasmon frequency at values of d_n less than critical point, and vice versa. There is a considerable value of ω_p even for undoped heterostructures.

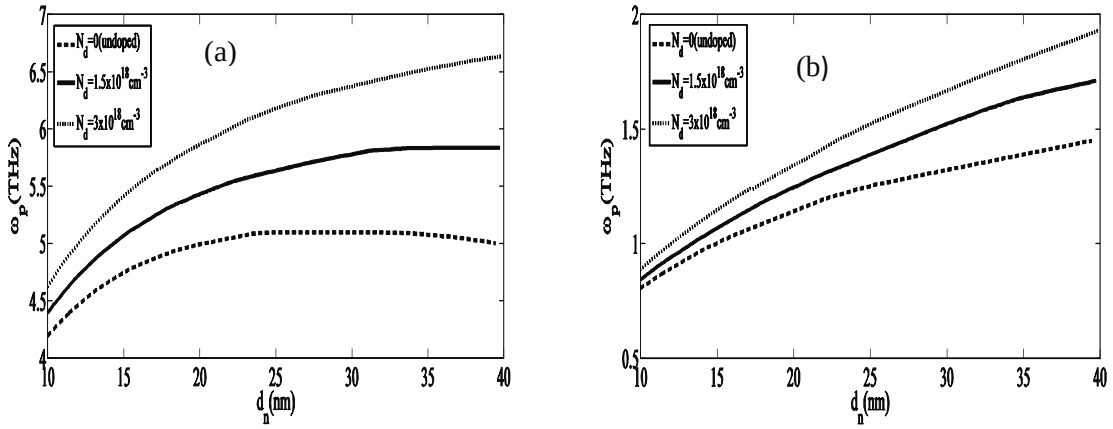

'Figure 7': Plasmon frequency vs barrier thickness at x=0.2, V_g=0, (a) L= 60 nm , (b) L=500 nm.

The change of plasmon frequency with doping concentration at different gate voltages is shown in 'figure 8'. We have smaller ω_p values when L=500 nm than L= 60 nm as it appears also in 'figures 6 and 7'.

'Figure 9' represents the dependence of plasmon frequency on the Al-mole fraction in the doped AlGaN layer at different gate voltages. The value of ω_p at L=60 nm is approximately twice its value at L=500 nm.

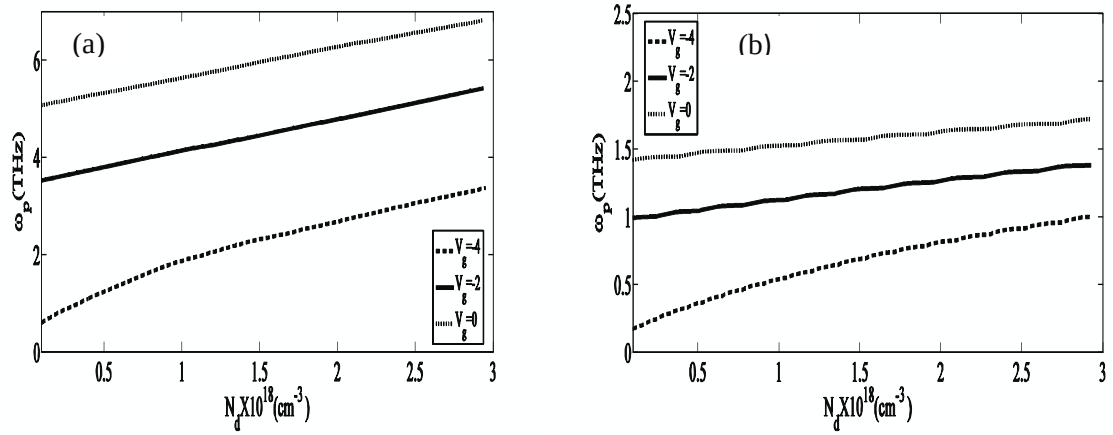

'Figure 8': Plasmon frequency vs doping density at x=0.2, d_n=25 nm, (a) L= 60 nm , (b) L=500 nm.

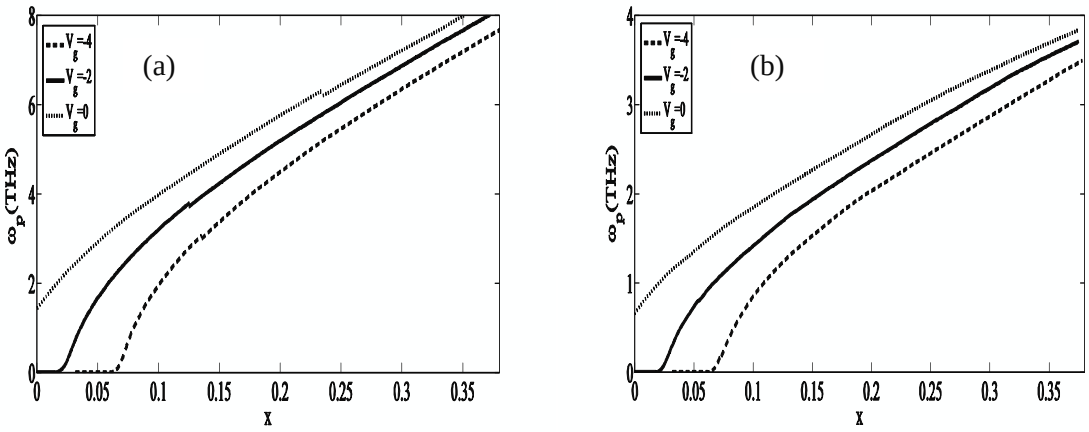

'Figure 9': Plasmon frequency vs Al-mole fraction at $N_d=2\times10^{18}cm^{-3}$, d_n=25 nm, (a) L= 60 nm , (b) L=500 nm.

Finally, the change of plasmon frequency with gate length is shown in 'figure 10'. The plasmon frequency increases with decreasing the gate length, but it should be noted that there are technical limitations in designing a HEMT plasmon device with very short gate length. Also, if the gate length is taken shorter and shorter, the ungated portion of the gate will increase.

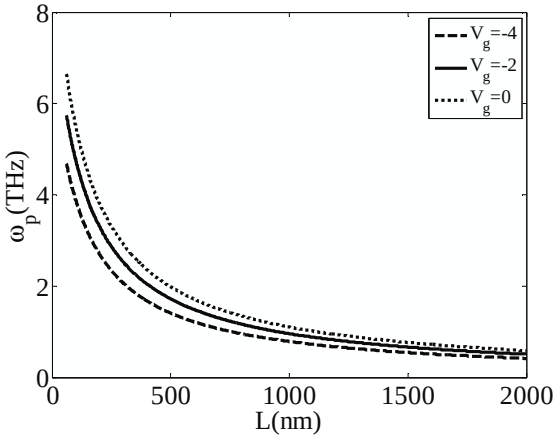

'Figure 10': Plasmon frequency vs gate length at x=0.25 and d_n=30.

The previous calculations of ω_p are taken for the fundamental plasmon mode (n=1) in a single-gated HEMT. To get higher frequencies we can consider higher order modes with n>1, but in this case, the dipole moment will decrease. It was suggested in [8] that to face this problem, a single-gated device is replaced by field effect transistors arrays.

The 2D plasma frequency can be measured by considering the THz absorption or emission spectra of a HEMT [8,26]. We compare our theoretical results with measurements taken in [26]. The emission absorption was measured for a HEMT of the following parameters: x=0.3, d_i=0, d_n=30 nm, N_d=0, L=250 nm, V_c= 4V. The position of the peaks in the emission spectra represents the plasmon frequency at different gate voltages. We use the same calculation method mentioned above to plot plasmon frequency with gate voltage in "figure 11". The circular points and the error bars at some gate voltages are taken from [26]. We notice a very good agreement of our calculations with experiment measurements.

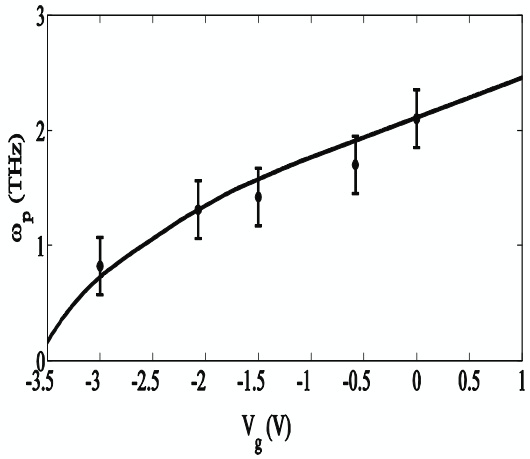

'Figure 11': Theoretical calculations of plasmon frequency vs gate voltage (solid curve) compared to experimental measurements taken from [26] (circular points with error bars: experimental measurements)

6. Conclusions

We have calculated the sheet charge density as a function of different transistor design parameters. We have found that the charge density for AlGaN/GaN HEMT is so high compared to other semiconductor heterostructures like AlGaAs/GaAs. This has many technical applications such as biosensors. The charge density increases with x, d_n, N_d, and V_g .

The plasmon frequency is directly proportional to N_s. We have found that it is possible to get frequencies from the GHz band up to 8 THz by choosing suitable HEMT parameters. If we desire to get higher mode frequencies, we should take into account the limitations on all previous parameters and gate length in the practical point of view. The accuracy of the optimized value of the plasmon frequency is controlled by taking into account the average position Δd of charge density in the channel.

We have found high sensitivity of the plasmon frequency to the gate voltage. This is important in fabrication of tunable THz plasma detectors and other THz devices. The results encourage using AlGaN/GaN heterostructure in such devices as a suitable choice. It is interesting to conclude that the structure produces this spectrum of plasma waves even with an undoped barrier, due to the large induced polarization of the heterostructure.

7. Acknowledgements

This work was funded by the EU Commission; the Erasmus Mundus External Cooperation Window (EM ECW) lot 2.

8. References:

[1] Rabbaa S, Vandermeiren W and Stiens J 2010 Longitudinal optical phonon-plasmon interaction in Ga-group V compounds for IR and THz applications *Proc. of the 15th Annual Symp. of the IEEE Photonics Benelux Chapter* (TU Delft: the Netherlands) pp 257-60.

[2] Liu L, Sensale-Rodriguez B, Zhang Z, Zimmermann T, Cao Y, Jena D, Fay P and Xing H 2010 Development of microwave and terahertz detectors utilizing AlN/GaN high electron mobility transistor *21st Int. Symp. on Space Terahertz Technology* (Oxford: England) pp 321-25.

[3] Dyakonov M and Shur M 1996 Plasma wave electronics: novel terahertz devices using two dimensional electron fluid *IEEE Trans. Electron Devices* 43 1640-45.

[4] Mustafa F and Hashim A 2010 Generalization 3D transverse magnetic mode method for analysis of interaction between drifting plasma waves in 2DEG-structured semiconductors and

electromagnetic space harmonic waves *Progress in Electromagnetics Research, PIER* **102** 315-335.
[5] Mustafa F and Hashim A 2010 Plasma wave electronics: a revival towards solid-state terahertz electron devices *J. Applied Sc.* **10** 1352-68.
[6] Popov V, Polischuk O and Shur M 2005 Resonant excitation of plasma oscillations in a partially gated two-dimensional electron layer *J. Appl. Phys.* **98** 033510.
[7] Hashim A, Hashizume T, Iizuka K and Hasegawa H 2003 Plasma wave interactions in the microwave to THz range between carriers in a semiconductor 2DEG and interdigital slow waves *Superlattice Microst* **34** 531-37.
[8] Popov V, Shur M, Tsymbalov G and Fateev D 2007 Higher-order plasmon resonances in GaN-based field-effect transistor arrays *Int. J. High Speed Electron. Syst* **17** 557-66.
[9] Hao Y, Yang L and Zhang J 2008 GaN-based semiconductor devices for terahertz *Terahertz Sci. Technol* **1** 51-64.
[10] Ryzhii V, Khmyrova I, Ryzhii M, Satou A, Otsuji T, Mitin V and Shur M 2007 Plasma waves in two-dimensional electron systems and their applications *Int. J. High Speed Electron. Syst* **17** 521-38.
[11] Stern F 1967 Polarizability of a 2-dimensional electron gas *Phys. Rev. Lett.* **18** 546.
[12] Grimes C and Adams G 1976 Observation of 2-dimensional plasmons and electron–ripplon scattering in a sheet of electrons on liquid-helium *Phys. Rev. Lett.* **36** 145-48.
[13] Allen S, Tsui D and Logan R 1977 Observation of 2-dimensional plasmon in silicon inversion layers *Phys. Rev. Lett.* **38** 980-83.
[14] Hiyamizu S, Saito J and Nanbu K 1983 Improved electron- mobility higher than 106 cm^2/Vs in selectively doped GaAs/n-AlGaAs heterostructures grown by MBE *Jpn. J. Appl. Phys., Part 2* **22** L609-11.
[15] Fiorentini V, Bernardini F and Ambacher O 2002 Pyroelectric evidence of nonlinear macroscopic polarization in III-nitride alloy heterostructures *Appl. Phys. Lett*. **80** 1204-06.
[16] Miller E, Yu E, Poblenz C, Elsass C and Speck J 2002 Direct measurement of the polarization charge in AlGaN/GaN heterostructures using capacitance-voltage carrier profiling *Appl. Phys. Lett*. **80** 3551-53.
[17] Ambacher O *et al* 1999 Two-dimensional electron gases induced by spontaneous and piezoelectric polarization charges in N- and Ga-face AlGaN/GaN heterostructures *J. Appl. Phys.* **85** 3222-33.
[18] Delagebeaudeuf D and Linh N 1982 Metal-(n) AlGaAs-GaAs two-dimensional electron gas FET *IEEE Trans. Electron Devices* **29** 955-60.
[19] Balkanski M and Wallis R 2000 *Semiconductor Physics and Applications* Oxford University Press Inc. (New York) pp 372-76.
[20] Shur M 1998 GaN based transistors for high power applications *Solid State Electron.***42** 2131-38.
[21] Yahyazadeh R and Hashempour Z 2010 The effect of depletion layer on the cut off frequency of AlGaN/GaN high electron mobility transistors *Proc. 27th Int. Conf. in Microelectronics (MIEL)* (Nis: Serbia) pp 165-68.
[22] Yakout M, AbdelRassoul R, AbdelFattah A and Essa S 2001 An accurate analytical model of the AlGaAs/GaAs high electron mobility transistor (HEMT) *18th National Radio Science Conf.* (Mansoura Univ.: Egypt) pp 531-39.
[23] Sen S, Pandey M, Khanna M and Gupta R 1997 A quasi two-dimensional analytical model for threshold voltage of a modulation doped field effect transistor *Asia Pacific Microwave Conf.* (Hong Kong: China) Vols I-III pp 705-08.
[24] Shey A and Ku W 1989 An analytical current-voltage characteristics model for high electron mobility transistors based on nonlinear charge-control formulation *IEEE Trans. Electron Devices* **36** 2299-306.

[25] Sun Y, Thompson S and Nishida T 2009 *Strain Effect in Semiconductors: Theory and Device Applications* Springer (New York) p 150.
[26] El Fatimy A *et al* 2010 AlGaN/GaN high electron transistors as a voltage-tunable room temperature terahertz sources *J. Appl. Phys.* **107** 024504.